Hindawi Publishing Corporation
Journal of Nanomaterials
Volume 2016, Article ID 4580518, 10 pages
http://dx.doi.org/10.1155/2016/4580518

Research Article

Effect of Growth Temperature and Time on Morphology and Gas Sensitivity of Cu_2O/Cu Microstructures

Ling Wu, Lun Zhang, Zhipeng Xun, Guili Yu, and Liwei Shi

College of Sciences, China University of Mining and Technology, Xuzhou City 221116, China

Correspondence should be addressed to Ling Wu; wlwlcumt@163.com and Lun Zhang; zhanglun05@163.com

Received 2 May 2016; Revised 25 July 2016; Accepted 23 August 2016

Academic Editor: Xin Zhang

A facile hydrothermal synthesis with $CuSO_4$ as the copper source was used to prepare micro/nano-Cu_2O. The obtained samples have been characterized by X-ray diffraction, scanning electron microscopy (SEM), and transmission electron microscopy (TEM). With increasing the reaction temperature and time, the final products were successively Cu_2O octahedron microcrystals, Cu_2O/Cu composite particles, and a wide range of Cu spherical particles. The gas sensitivity of products towards ethanol and acetone gases was studied. The results showed that sensors prepared with Cu_2O/Cu composites synthesized at 65°C for 15 min exhibited optimal gas sensitivity. The gas sensing mechanism and the effect of Cu in the enhanced gas response were also elaborated. The excellent gas sensitivity indicates that Cu_2O/Cu composites have potential application as gas sensors.

1. Introduction

Cu_2O, a famous p-type semiconductor material, has recently attracted extensive interests owing to the widespread applications in solar energy conversion, photocatalysts, sensors, and lithium ion batteries [1–4], so the preparation of Cu_2O nanoparticles has become a very popular topic in the field of scientific research. Up to now, many different methods of synthesizing Cu_2O micro/nanocrystals have been reported [5–15]. Among the various synthesis methods, hydrothermal synthesis is often used by plenty of researches because some versatile morphologies and different phases are easy to get by tuning the reaction elements, such as the growth temperature and duration time. However, such reports were mainly devoted to morphology evolution and the photocatalytic activities of Cu_2O micro/nanoparticles, while the gas sensitivities of sensors based on Cu_2O or Cu_2O-based hybrids such as Cu_2O/Cu composite had seldom been investigated. Gas sensors, especially metal oxide semiconductor materials, have aroused most interests due to their advantages of high response and short recovery time in the detection of environmental pollution, various harmful gases, industrial wastes, and so forth. It is generally believed that the sensing mechanism of metal oxide semiconductor sensor is mainly involving the modulation performance to the conduction of semiconductor performed by gas molecules adsorbed on the surface of sensors. That is, the surface conductive characteristics of oxide semiconductor will significantly change before and after the gas molecules adsorption; and adsorption of different gas molecules will lead to the different changes of conductivity. Moreover, the morphologies, species, and the production process of materials have a great influence on the sensitivity of sensors. To enhance the sensing properties of gas sensors, some efforts have been devoted to the synthesis of some various hollow or porous structures [16–20] or to the incorporation with precious metals, such as Au [21, 22] and Ag [23, 24]. During the past ten years, some semiconductor oxides, such as SnO_2 [20, 25–27], ZnO [28–30], In_2O_3 [31, 32], and WO_3 [33–36], have been intensively investigated. However, the performance and fundamental understanding of micro/nano-Cu_2O-based sensors are still in the elementary stages. In the field of gas-sensing, Cu_2O crystal has great potential applications in detecting pollutant gases considering its low cost and significant surface reactivity with both reducing and oxidizing gases, and further investigations are very necessary to improve the theory of gas sensitivity of Cu_2O crystals.

Table 1: The crystal structure and morphology of samples synthesized at different condition.

Samples	Temperature (°C)	Time (min)	Product	Morphology
S1	20	30	Cu_2O	Octahedral
S2	65	15	Cu_2O/Cu	Octahedral/sphere
S3	65	30	Cu	Solid/hollow sphere
S4	80	9	Cu	Sphere
S5	80	30	Cu	Sphere

In this paper, Cu_2O micro-octahedron, micro/nano-Cu_2O/Cu composite particles, and Cu spherical particles were obtained with a facile one-pot solution synthesis only by controlling the reaction temperature and time. The influences of reaction temperature and time on the morphologies and phases of the products were investigated. Acetone and ethanol gases were selected to be the probe analytes to detect the gas sensitivity of products.

2. Experimental Details

2.1. Synthesis of Cu_2O, Cu_2O/Cu, and Cu Microstructures. In our facile one-pot experiment, cupric sulfate ($CuSO_4$) was used as the Cu^{2+} source and PVP as the soft template. In the preparation, 0.16 g $CuSO_4$ was dissolved into 100 mL deionized water under continuous magnetic stirring. Then 0.18 g PVP was added into the above solution under continuous stirring for about 10 min. In sequence, 25 mL (0.06 M) NaOH solution was added into the above solution, and then the color of the solution turned to light blue from clarification. After full stirring, 2 mL hydrazine hydrate solution prepared in advance was added dropwise as the reducing agent. The solution was then kept at 65°C in a water bath until numerous reddish brown particles appeared. After that, it was cooled to the room temperature naturally and then the final products were separated by centrifugation and cleaned four times by filtration with plenty of deionized water and pure ethanol. Finally, the products were dried in a vacuum oven at 60°C for 4 h. The obtained sample at this temperature was named sample 1 (S1). Adjusting the water bath temperature and time, samples 2–5 (S2–S5) were achieved correspondingly. The following procedure was the same as that of S1.

2.2. Fabrication and Measurement of Gas Sensors. The fabrication process of the gas sensor was similar to that reported before by Wan and was briefly described [37]: The products were dispersed in a suitable amount of deionized water to form a paste. Then the paste was coated uniformly on the external surface of the ceramic tube with Au electrodes and Pt wires. To keep the sensor working at elevated temperature, a Ni–Cr coil heater was inserted into the tube to form an indirect-heated gas sensor. The sample was suspended with Pt wires to form a heat insulation structure. Desired constant operating temperatures could be obtained by applying certain voltages to the heater. The substrate temperature was measured with a thermocouple. The responses of gas sensors in dry air were tested by the gas distribution method. The gas-sensing properties were tested in a steel chamber through which a controlled atmosphere was allowed to flow. The electrical response of the sensor was measured with an automatic test system controlled by personal computer and a typical testing procedure. The electrical properties of the gas sensor were measured by a WS-60A gas-sensing characterization system (Weisheng Instruments Co. Ltd., China). A square voltage signal (3.5 V and 0.4 Hz) was applied to the sensor heating resistor. The gas sensitivity is defined as $S = R_{gas}/R_{air}$, where R_{gas} and R_{air} are the resistances of the sensors in analyte gas and in ambient air when the sensor was heated, separately.

2.3. Characterization. The crystal structures of the as-prepared samples were identified by X-ray powder diffraction (XRD) using an advanced X-ray diffractometer (D8 ADVANCE, Bruker, Germany) with Cu-Kα radiation operating at 40 kV and 30 mA. The morphology and size were investigated by field emission scanning electron microscopy (FESEM; S4800 and Hitachi, Japan) at an accelerating voltage of 5 kV. The inner microstructure of the samples was studied by transmission electron microscopy (TEM) and high-resolution TEM (HRTEM) (Tecnai G2 F20, FEI, USA) at an accelerating voltage of 200 kV. The N_2 adsorption-desorption isotherms of the products were measured at 77 k on Specific Surface Area Analyzer Belsorp-max (BELSORP-max ver. 2.1, Japan). The Brunauer-Emmett-Teller (BET) specific surface area (SBET) was determined by a multipoint BET method. The samples to be tested were measured at the same condition simultaneously. Before the BET measurement, heat treatment has been done firstly at 120°C for 4 h under the vacuum condition of $1.292E-8$ Pa. Then at the saturated liquid nitrogen temperature 77 K and the vacuum degree of 10^{-7} mmHg, nitrogen adsorption and desorption (BET) measurements were performed at a relative pressure P/P_0 (P, P_0, resp., represent the equilibrium pressure of nitrogen adsorption at low temperature and saturation pressure) range of 0.4–1.0. Through analysis of the adsorption-desorption isotherms, specific surface area can be calculated by the multipoint BET method.

3. Results and Discussion

3.1. Crystal Structure and Morphology. Firstly, the effects of reaction condition on the crystal structure and morphology of samples were examined, which is shown in Table 1. It can be seen that the crystal structures and morphologies of the as-prepared samples are significantly influenced by the reaction temperature and time.

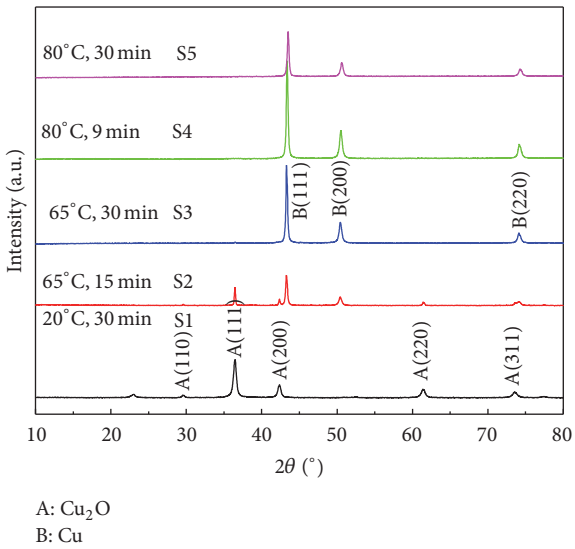

FIGURE 1: XRD patterns of samples synthesized at different reaction temperature for various time.

Figure 1 shows the XRD patterns of Cu_2O, Cu_2O/Cu, and Cu microstructures prepared at different reaction conditions. In order to collect reliable data to investigate the growth mechanism, the morphology and structure of synthesized particles are also studied by SEM and TEM measurements and the results are presented in Figure 2. High-resolution TEM (HRTEM) as shown in Figure 2 was also used to investigate the inner ultrafine structure of S1~S5, in order to study the influence of morphology on the gas response activity that will be discussed later. When the hydrothermal reaction was carried out at 20°C for 30 min, pure Cu_2O (S1) was detected from the XRD results. All the characteristic diffraction peaks were labeled and can be indexed according to the cubic phase for Cu_2O (JCPDS card no. 5-667). Obviously, no other diffraction peaks related to impurities such as CuO or Cu could be detected. Figures 2(a) and 2(b) presented the SEM and TEM images of products synthesized at this reaction condition. The products consist of uniformly well-defined octahedral structure with an average edge length estimated to be about 800 nm. And it was observed that Cu_2O octahedral was solid and no hollow structure was found. HRTEM image (Figure 2(b1)) showed obviously that the surface of octahedral particle was not smooth, which has been piled up by approximately 5 nm ultrafine particles like fish scales (also shown in Fig. S(1) of Supplementary Material available online at http://dx.doi.org/10.1155/2016/4580518). The structure causes the specific surface area of S1 to increase greatly. Moreover, the lattice fringes of the "fish scale" have interplanar spacing of 0.244 nm, which is corresponding to the cubic Cu_2O (111) plane [11].

While the reaction condition was changed to 65°C for 15 min, it was found that the (111) and (200) planes from Cu (JCPDS card no. 4-836) appeared in addition to those of Cu_2O in Figure 1. Along with the appearance of Cu diffraction peaks, the intensities of the (111) and (110) peaks from Cu_2O significantly decreased, indicating the reductive conversion from Cu_2O to Cu. From SEM and TEM results, some nonuniformly spherical structures were observed in Figures 2(c) and 2(d). In addition, a small part of octahedral structures with rough surfaces were also observed, which would be inclined to dissolve into many small spherical particles. Moreover, Figure 2(d1) exhibits that sample S2 has special nanocluster structures that are made up of ultrafine grains with the sizes of 2–7 nm. The HRTEM images showed that the clearly resolved interplanar distances of Cu_2O and Cu were d_{111} = 0.247 nm and d_{111} = 0.209 nm, respectively [38, 39], which can be also seen in Fig. S(2) in Supplementary Information. When the reaction time was extended to 30 min at the same temperature, the phase and purity of the products were confirmed in Figure 1 (S3), and no characteristic peaks of CuO or Cu_2O were detected, indicating that Cu_2O was further reduced to Cu. Parallel to the further hydrothermal reduction from Cu_2O to Cu, the octahedral structure disappeared completely and some part of hollow spherical structure appeared which was built up by numerous small nanoparticles shown in Figure 2(e). In addition, some solid nanospheres were also found in Figures 2(e) and 2(f). At 65°C, the longer the reaction time, the stronger and sharper the diffraction peaks of Cu phase. The regular spacing of the lattice plane of the hollow spherical particle is calculated to be 0.209 nm in Figure 2(f1), in good agreement with the (111) lattice spacing of metal Cu [39]. When reaction temperature was raised to 80°C (the products were labeled as S4 and S5 for 9 min and 30 min, resp.), even only for 9 min, the XRD results showed that only Cu diffraction peaks were found. This suggested that higher temperature in the reaction system could accelerate the phase transformation from Cu_2O to Cu. And SEM images of product shown in Figures 2(g) and 2(h) present irregular spherical shape. When the reaction time was prolonged to 30 min, the similar structure can be found except the smaller and smoother particles in Figures 2(i) and 2(j). Nevertheless, it was found that the diffraction peaks of Cu got weakened when extending the reaction time at 80°C. It might be attributed to the decrease in the size of Cu particles with prolonging the reaction time, as would be observed in SEM images. It is clear that surfaces of the spherical particles in Figures 2(h1) and 2(j1) are not smooth. The distinct crystal lattices illustrate that S4 and S5 possess good crystalline structure [40]; the distinct lattice fingers with d spacing were, respectively, 0.209 and 0.210 nm corresponding to the (111) lattice plane of Cu, which is in good agreement with that obtained by XRD shown in Figure 1.

3.2. Possible Growth Mechanism. From the above analysis, the growth temperature and duration time are the determined factors for the phases and morphologies of final products. When the growth temperature is lower than 20°C, $Cu(OH)_2$ precursor was formed firstly at the outside of the micelle, which can be clearly deduced from the light blue solution after NaOH solution was added, and then $Cu(OH)_2$ was reduced to Cu_2O octahedral microcrystals seen in Figures 2(a) and 2(b) by hydrazine hydrate (PVP) which is a common reduction agent. And the related chemical reaction for Cu^{2+}

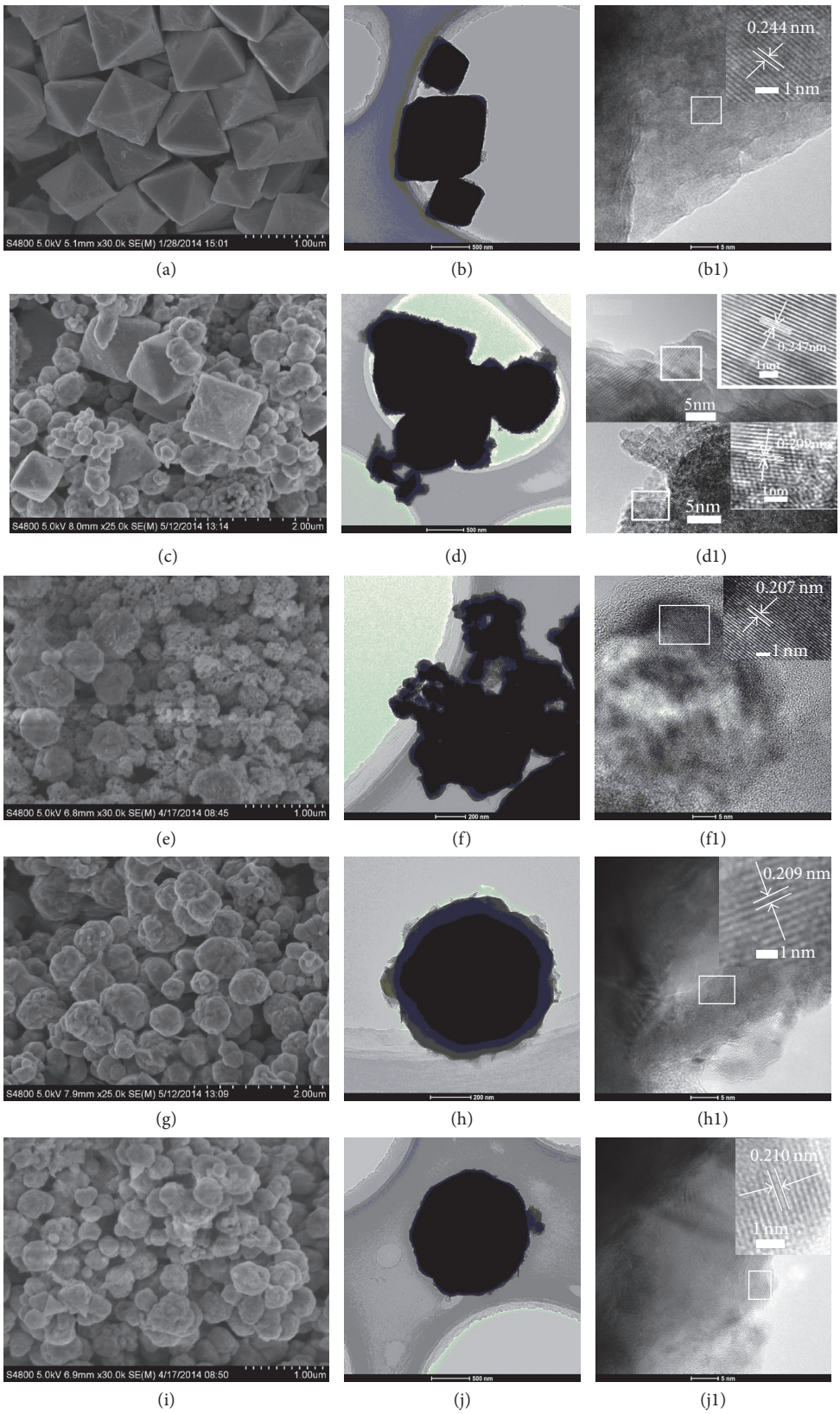

Figure 2: SEM images (column 1), TEM images (column 2), and HRTEM images (column 3) of different samples, with the inserts corresponding to the white marked regions. Lines 1–5 corresponding to samples S1–S5.

reduction by $N_2H_4{\cdot}H_2O$ which was consistent with the reported research was proposed as follows [41]:

$$Cu^{2+} + 2(OH)^- \longrightarrow Cu(OH)_2 \quad (1)$$

$$4Cu(OH)_2 + N_2H_4 \longrightarrow 2Cu_2O + 6H_2O + N_2 \quad (2)$$

Higher temperature can accelerate the reaction rate; when the hydrothermal reaction was carried out at 65°C for 15 min, most of octahedral particles began to collapse and dissolve to form irregular spherical particles in Figures 2(c) and 2(d). Along with the morphology evolution from the octahedral structure to spherical one, Cu_2O phase is partly reduced into Cu during the process that has been proved by XRD patterns in Figure 1 and the HRTEM images in Figure 2(d1). It is clear that the produced Cu nanoparticles with the size about 2–7 nm were distributed on the surface of the Cu_2O particles in Fig. S(2). It was deduced from similar reduction reported before that the reaction equation in alkaline environment in this process was proposed as follows [15, 42]:

$$4Cu^+ + N_2H_4 + 4(OH)^- \longrightarrow 4Cu + 4H_2O + N_2 \quad (3)$$

As expected, the content of Cu in the Cu_2O/Cu composite increased with increasing the reaction time to produce a range of composites with controllable composition. It had been proved that the reduction efficiency increased with the increase of time [15, 43]. That had also been proved by Fig. S(2) in Supplementary Material, in which the content of Cu increased with the extension of time. Prolonging the reaction time, the further reduction according to (3) happened. When the duration is extended to 30 min at 65°C, only Cu diffraction peaks were displayed in XRD patterns. Parallel to the reduction conversion of Cu_2O to Cu, octahedral particles disappeared and hollow structure appeared. Morphology evolution related to this process presented two possibilities: one was the fact that the small particles continue to grow up with Ostwald ripening mechanism, and the other was the fact that hollow structure was firstly aggregated by small particles according to certain rule and then gradually grew into solid construction with growth time.

When hydrothermal temperature was 80°C, the final products were all pure Cu even only for 9 min. It was thought that there were also two feasibilities for the reduction process. One was the fact that the Cu^+ ions were converted into Cu via further reduction according to chemical equation (3), which could be accelerated at higher temperature, and another may be the direct phase transformation from Cu^{2+} to Cu, and the following reactions occur:

$$2Cu^{2+} + N_2H_4 + 4(OH)^- \longrightarrow 2Cu + 4H_2O + N_2 \quad (4)$$

The whole reaction process can be concluded: (1) reductive transformation from Cu^{2+} to produce octahedral Cu_2O, (2) further reductive transformation from Cu_2O to Cu to produce Cu_2O/Cu composite microstructure with increasing temperature and reaction time, and (3) Cu_2O being totally reduced into pure Cu or the rapid direct phase transition from Cu^{2+} to Cu. The strong reaction condition dependence on products can also be demonstrated in Table 1. With increasing temperature and time, the solubility of precursor increases; then the more stable morphology (from octahedral structure to spherical one) and crystal (from Cu_2O to Cu) gradually formed with further strengthened reduction reaction, while the particle size decreased in general with the rising temperature; that is probably because the nucleation rate is faster than grain growth speed.

3.3. Gas Sensitivity. As is well known, multicomponent composites comprising different types of materials offer novel properties and are quite attractive due to their potential applications in lithium-ion batteries, diluted magnetic semiconductors, optoelectronic devices, and photocatalysis [11, 44–46]. However, most strategies available for synthesizing metal-semiconductor hybrid structures often require multistep and complex procedures. So the formation of well-controllable hybrid structures has been still a great challenge. It is worth mentioning from the above discussions that Cu_2O/Cu composites were synthesized by facile one-pot solution synthesis and it supplied a simple and effective method for design of metal-semiconductor hybrid structures.

From the above discussion, S2 and S3 in Figures 2(c) and 2(e) exhibit hollow structures partly. Hollow structure is suitable to gas sensing due to pore structure and larger surface area. In order to determine the absorptive property, nitrogen adsorption and desorption (BET) measurements were performed on both products seen in Figure 3(a). At a relative pressure (P/P_0) range of 0.4–1.0, both samples exhibited the type H3 hysteresis loops indicating the presence of slit-like mesoporous material (2–50 nm) in both samples. The BET specific surface areas of S2 and S3 were 8.25 and 7.88 $m^2 g^{-1}$, respectively. It is well known that operating temperature and gas concentration have great influence on gas sensor response. Herein, the response of all sensors at different operating temperature was tested simultaneously with gas consideration in a range of 10–500 ppm under identical experimental conditions. Figure 3(b) showed the responses curves of S2 and S3 towards 100 ppm acetone gas at different operating temperature. In order to be more accurate, four gas sensors were made by each sample. The data of the average sensitivity of the four sensors were exhibited and the standard deviation from the mean value was also marked by error bar on Figure 3(b). It can be seen that the responses of sensors were strongly dependent on the operating temperature, especially for S2-based sensor. Comprehensively considering economy and efficiency, 250°C was selected as the working temperature to carry on the research of gas sensitivity.

Figure 4(a) exhibited the typical dynamic response and recovery curves of all samples when cycled by increasing ethanol vapor in a range of 10–500 ppm and at the working temperature of 250°C simultaneously. Similar to what was previously reported [37], as a p-type gas sensor, the resistance underwent different increases on the injection of reducing gases (ethanol) and then recovered its initial value quickly after gas was released, indicating that each of gas sensor test devices responded as expected for p-type semiconductors and was sensitive to ethanol. With the increase of ethanol concentration, the peak becomes stronger, suggesting that

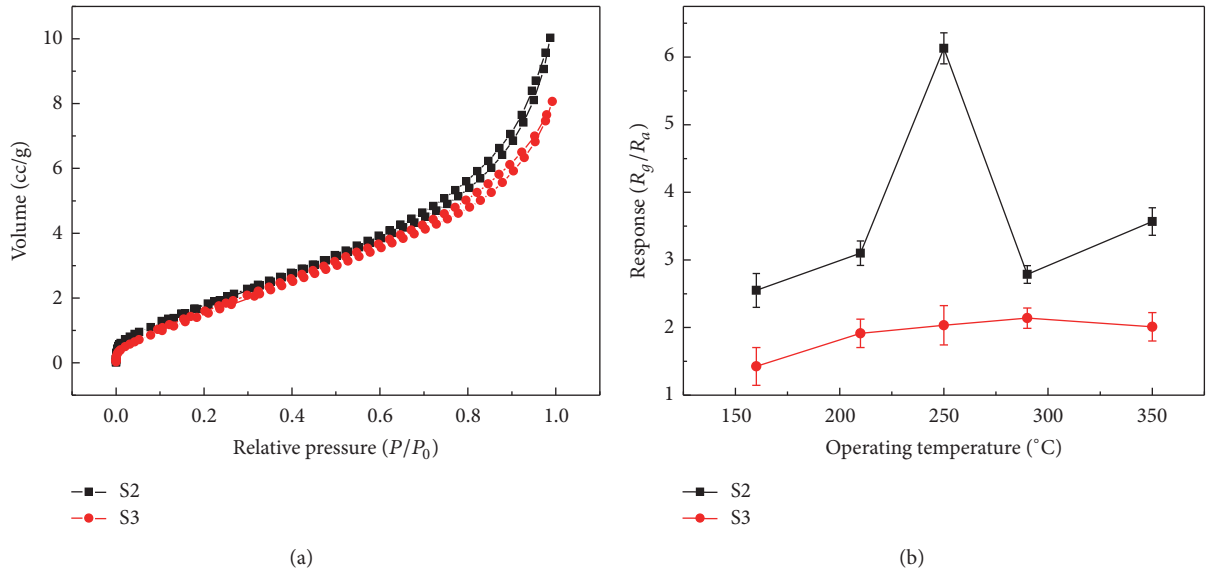

FIGURE 3: (a) Typical N_2 adsorption-desorption isotherms of the representative samples; (b) the responses of sensors to 100 ppm acetone gas as a function of operating temperature.

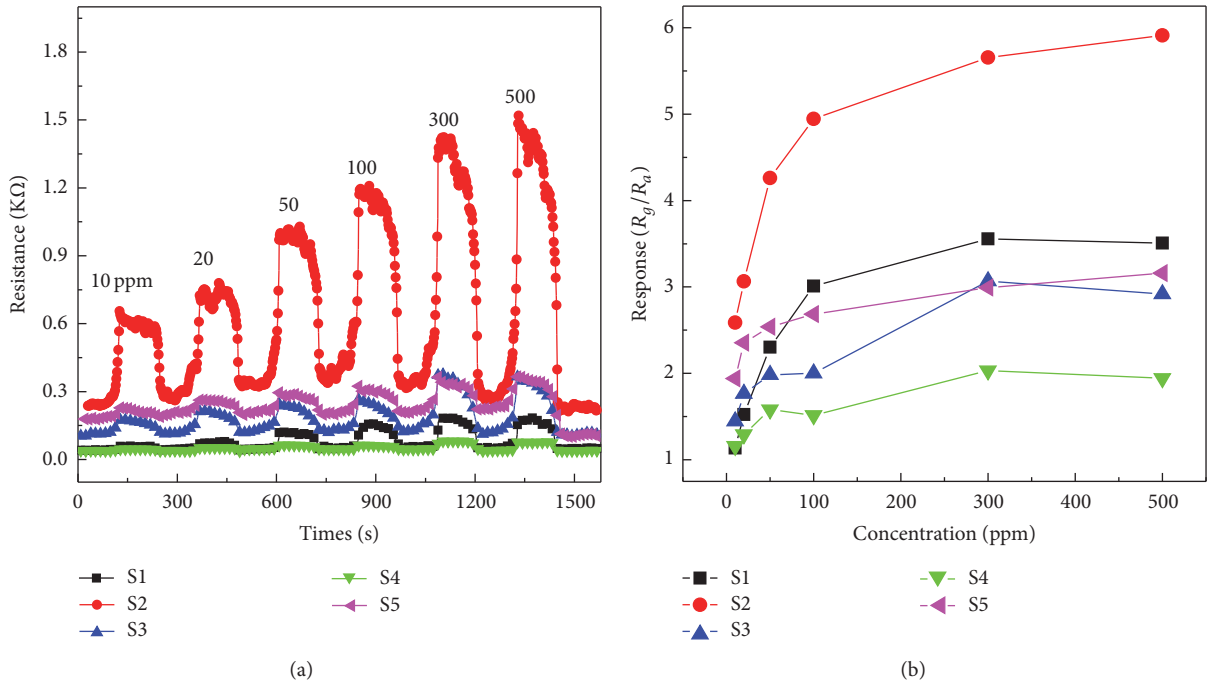

FIGURE 4: (a) Dynamic response-recovery curves of the gas sensors at 250°C. (b) Response (R_g/R_a) versus ethanol concentration for the gas sensors.

the ethanol sensors based on samples are sensitive to the concentration of ethanol. Particularly, the response amplitude of Cu_2O/Cu composite-based sensor was much larger than pure Cu_2O octahedral or Cu microsphere, indicating a promotion effect of Cu_2O/Cu composite on gas sensitivity. Figure 4(b) showed the relationship between gas response and the ethanol concentration. Corresponding to the result displayed in Figure 4(a), the gas sensor prepared with S2 showed excellent sensitivity to ethanol gas. It was also clearly illustrated that the sensitivity increased rapidly at first (below 100 ppm) and then slowly in the range of 100–500 ppm. Particularly, the response of S1 sensor increased from 1.13 to 3.01 with the ethanol concentration from 10 to 100 ppm, which was faster than those of S3, S4, and S5 samples. That is because the scale-like surface structure of S1 in Figure 2(b1) and Fig. S(2) can increase the contact areas of test gas.

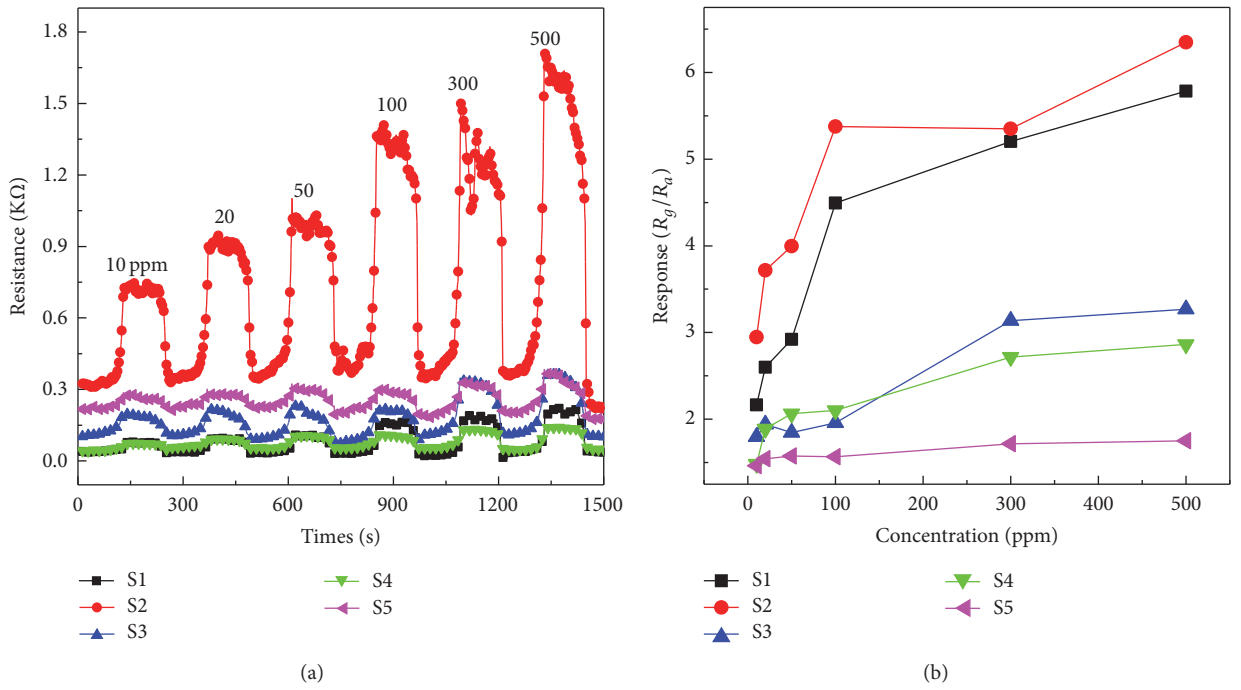

FIGURE 5: (a) Dynamic response-recovery curves of the gas sensors at 250°C. (b) Response (R_g/R_a) versus acetone concentration for the gas sensors.

Furthermore, the changes of resistance of Cu microparticles of S3–S5 are mainly due to physical absorption because of unsmooth surface. When the gas concentration is higher than 100 ppm, the sequence of sensitivity is as follows: S2 > S1 > S5 > S3 > S4. Moreover, the response and recovery time of Cu_2O/Cu composite-based sensor were 11 and 26 s, respectively, which are shorter than 15 and 30 s of Cu_2O reported by Zhang et al. [3]. Thus it can be deduced that incorporation of Cu with semiconductor can improve the gas sensing properties.

Although ethanol gas sensors performances have been widely studied [47–51], very few researches on acetone sensor had been reported. Among the common environmental pollutants, acetone is a kind of well-known combustible hazardous chemical. And it is toxic to human body, which forces anesthetic action on the central nervous system. Thus, effective acetone gas sensors with rapid response and high sensitivity are of great importance and much needed for both environmental protection and human health. So the sensing performances to acetone gas were given in Figures 5(a) and 5(b). Similar to the sensing test results towards ethanol, the resistances of all sensors increased to different extents on exposure to acetone vapor and then resumed when releasing the test gas. The response and recovery time of the Cu_2O/Cu composite-based sensors were about 20 and 30 s, respectively, which are shorter than those of the other sensors. Moreover, gas sensor based on S5 showed lower sensitivity to acetone compared to ethanol gas, indicating that S5 exhibits selectivity to ethanol.

The widely accepted sensing mechanism of metal oxide is based on the modulation of the depletion layer by oxygen absorption. When oxidizing molecules are adsorbed onto an n-type oxide surface, a depletion layer is formed in response, resulting in the increase of the sensor resistance. The reverse happens to a p-type gas sensor; that is, oxidizing gases will induce an accumulation of holes near the surface resulting in a decrease in resistance, while reducing gases, on the other hand, will deplete holes near the surface, resulting in an increase in resistance [37–52]. So in the experiment, when the sensor is being exposed to air, a certain amount of O_2 can be adsorbed on the surface of Cu_2O particles. Then ionization from O_2 at the semiconductor surface into O_2^-, O^{2-}, or O^- ions appeared by capturing electrons from the conduction band of Cu_2O, which results in an accumulation layer of holes near the surfaces of metal oxides and the decrease of surface resistance. When a reductive gas is introduced, like ethanol, a chemical reaction takes place between C_2H_5OH and O_2^-, O^{2-}, and O^- (O^- species are dominant at the operating temperature [49]), which results in relatively strong activation on the surface of the Cu_2O sensor:

$$\begin{aligned}(C_2H_5OH)_{(ads)} + 7O^-{}_{(ads)} \\ \longrightarrow 2CO_{2(gas)} + 3H_2O_{(gas)} + 7e^-\end{aligned} \quad (5)$$

According to the above equation, the electrons are released and recombined with holes, which result in a lower carrier concentration and an increase of the resistance.

Previous work reported that the incorporation of precious metals such as Pd, Pt, or Au with semiconductor oxides is an effective way to improve gas sensing properties [21, 47, 51–55]. Although the sensitivity of gas sensors based on pure Cu_2O

micro/nanoparticles and composite of Cu_2O with metals such as Au had been reported [3, 22, 56], as far as we know, the sensitivity of composite of Cu_2O/Cu micro/nanoparticles has seldom been studied. Herein, a facile in situ method was used for the growth of Cu nanoparticles by hydrothermal reductive transformation directly on the surfaces of Cu_2O seen in Figure 2(d1). Comparing with sputtering, impregnation, and other surface modification techniques, in situ growth methods have exhibited the advantages of avoiding introduction of impurities. Gas-sensing studies above indicate that the sensitivity of Cu_2O/Cu composite toward ethanol and acetone showed improved response at any given concentration. The enhanced sensing performance is due to the sensitization catalysis of Cu nanoparticles that has been proposed via a "spill-over effect" [22, 57]; that is, Cu nanoparticles activate the target gas by dissociation and subsequent spill-over of dissociation fragments onto the gas sensing material, which causes the gas response. In the Cu_2O/Cu composite gas sensor, Cu particles increase the molecule to ion conversion rate and the quantity of adsorbed oxygen; as a result, a deeper depletion layer is formed compared to the pure Cu_2O. When ethanol or acetone gas is introduced, the layer would decrease or disappear rapidly, resulting in a dramatic change in the conductivity of semiconductor materials. In a word, Cu particles increase both the quantity of oxygen species and the molecule-ion conversion rate, thus significantly enhancing the ethanol and acetone sensing properties.

So it can be deduced that incorporation of Cu with semiconductor oxides was an effective way to improve the gas sensing properties, which is in accordance with what was reported in the previous work [21, 47, 51–55]. Considering the low-cost and facile synthesizing method of the Cu_2O/Cu composite, they are emerging as one of the most potential candidates for gas sensors in the field of gas sensing.

4. Conclusions

In summary, through a facile hydrothermal reduction, we have successfully realized the phase transformation from Cu_2O octahedral into Cu_2O/Cu composite and then a wide range of novel Cu microspheres by simply changing reaction temperature and duration time. The gas sensing properties of Cu_2O/Cu composite that have seldom been studied towards acetone and ethanol are investigated here. The results show that Cu_2O/Cu composite exhibited higher sensitivity than those of other samples. The reason is mainly due to the Cu particles serving as sensitizers or promoters, which could increase the conversion rate of molecule to ion and the quantity of adsorbed oxygen. The excellent gas sensitivity and low economic cost indicate that Cu_2O/Cu composite has potential application as gas sensors.

Competing Interests

The authors declare that they have no competing interests.

Acknowledgments

This work was supported by the National Natural Science Foundation of China (Grants nos. 11204371, 11304377, and 11304378) and the project from "College Student Innovation Fund" under Grant no. 20160241-CUMT.

References

[1] R. P. Wijesundara, L. D. R. D. Perera, K. D. Jayasuriya et al., "Sulphidation of electrodeposited cuprous oxide thin films for photovoltaic applications," *Solar Energy Materials and Solar Cells*, vol. 61, no. 3, pp. 277–286, 2000.

[2] B. White, M. Yin, A. Hall et al., "Complete CO oxidation over Cu_2O nanoparticles supported on silica gel," *Nano Letters*, vol. 6, no. 9, pp. 2095–2098, 2006.

[3] J. Zhang, J. Liu, Q. Wang, and Y. D. Li, "Nearly monodisperse Cu," *Chemistry of Materials*, vol. 18, no. 4, pp. 867–871, 2006.

[4] P. Poizot, S. Laruelle, S. Grugeon, L. Dupont, and J. Tarascon, "Nano-sized transition-metal oxides as negative-electrode materials for lithium-ion batteries," *Nature*, vol. 407, no. 6803, pp. 496–499, 2000.

[5] J. A. Eastman, S. U. S. Choi, S. Li, W. Yu, and L. J. Thompson, "Anomalously increased effective thermal conductivities of ethylene glycol-based nanofluids containing copper nanoparticles," *Applied Physics Letters*, vol. 78, no. 6, pp. 718–720, 2001.

[6] K. J. Ziegler, R. C. Doty, K. P. Johnston, and B. A. Korgel, "Synthesis of organic monolayer-stabilized copper nanocrystals in supercritical water," *Journal of the American Chemical Society*, vol. 123, no. 32, pp. 7797–7803, 2001.

[7] Z. Liu, Y. Yang, J. Liang et al., "Synthesis of copper nanowires via a complex-surfactant-assisted hydrothermal reduction process," *Journal of Physical Chemistry B*, vol. 107, no. 46, pp. 12658–12661, 2003.

[8] L. Wang, T. Fei, Z. Lou, and T. Zhang, "Three-dimensional hierarchical flowerlike α-Fe_2O_3 nanostructures: synthesis and ethanol-sensing properties," *ACS Applied Materials and Interfaces*, vol. 3, no. 12, pp. 4689–4694, 2011.

[9] S. Q. Tian, D. W. Zeng, X. L. Peng, S. P. Zhang, and C. S. Xie, "Processing-microstructure-property correlations of gas sensors based on ZnO nanotetrapods," *Sensors and Actuators B: Chemical*, vol. 181, pp. 509–517, 2013.

[10] M. Hara, T. Kondo, M. Komoda et al., "Cu_2O as a photocatalyst for overall water splitting under visible light irradiation," *Chemical Communications*, vol. 29, pp. 357–358, 1998.

[11] C. Huang, Z. Long, M. Miyauchi, and X. Qiu, "A facile one-pot synthesis of Cu-Cu_2O concave cube hybrid architectures," *CrystEngComm*, vol. 16, no. 23, pp. 4967–4972, 2014.

[12] D. Rehnlund, M. Valvo, C.-W. Tai et al., "Electrochemical fabrication and characterization of Cu/Cu_2O multi-layered micro and nanorods in Li-ion batteries," *Nanoscale*, vol. 7, no. 32, pp. 13591–13604, 2015.

[13] M. Zahmakiran, S. Özkar, T. Kodaira, and T. Shiomi, "A novel, simple, organic free preparation and characterization of water dispersible photoluminescent Cu_2O nanocubes," *Materials Letters*, vol. 63, no. 3-4, pp. 400–402, 2009.

[14] H. Yang and Z.-H. Liu, "Facile synthesis, shape evolution, and photocatalytic activity of truncated cuprous oxide octahedron microcrystals with hollows," *Crystal Growth and Design*, vol. 10, no. 5, pp. 2064–2067, 2010.

[15] S. Dehghanpour, A. Mahmoudi, M. Mirsaeed-Ghazi, N. Bazvand, S. Shadpour, and A. Nemati, "Cu_2O microsphere, microspherical composite of Cu_2O/Cu nanocrystals and various Cu microcrystals: in situ hydrothermal conversion of Cu-aminodiphosphonate complexes," *Powder Technology*, vol. 246, pp. 148–156, 2013.

[16] J. H. Lee, "Gas sensors using hierarchical and hollow oxide nanostructures: overview," *Sensors and Actuators B*, vol. 140, no. 1, pp. 319–336, 2009.

[17] J. Huang, N. Matsunaga, K. Shimanoe, N. Yamazoe, and T. Kunitake, "Nanotubular SnO_2 templated by cellulose fibers: synthesis and gas sensing," *Chemistry of Materials*, vol. 17, no. 13, pp. 3513–3518, 2005.

[18] F. Song, H. L. Su, J. J. Chen, W. J. Moon, W. M. Lau, and D. Zhang, "3D hierarchical porous SnO," *Journal of Materials Chemistry*, vol. 22, no. 3, pp. 1121–1126, 2012.

[19] F. Song, H. Su, J. Han, W. M. Lau, W.-J. Moon, and D. Zhang, "Bioinspired hierarchical tin oxide scaffolds for enhanced gas sensing properties," *Journal of Physical Chemistry C*, vol. 116, no. 18, pp. 10274–10281, 2012.

[20] S. Tian, X. Ding, D. Zeng, J. Wu, S. Zhang, and C. Xie, "A low temperature gas sensor based on Pd-functionalized mesoporous SnO_2 fibers for detecting trace formaldehyde," *RSC Advances*, vol. 3, no. 29, pp. 11823–11831, 2013.

[21] X. Wang, S. Qiu, C. He, G. Lu, W. Liu, and J. Liu, "Synthesis of Au decorated SnO_2 mesoporous spheres with enhanced gas sensing performance," *RSC Advances*, vol. 3, no. 41, pp. 19002–19008, 2013.

[22] X.-W. Liu, F.-Y. Wang, F. Zhen, and J.-R. Huang, "In situ growth of Au nanoparticles on the surfaces of Cu_2O nanocubes for chemical sensors with enhanced performance," *RSC Advances*, vol. 2, no. 20, pp. 7647–7651, 2012.

[23] X. Liu, Z. Chang, L. Luo, X. Lei, J. Liu, and X. Sun, "Sea urchin-like Ag-α-Fe_2O_3 nanocomposite microspheres: synthesis and gas sensing applications," *Journal of Materials Chemistry*, vol. 22, no. 15, pp. 7232–7238, 2012.

[24] Z. Zhang, H. Song, S. Zhang et al., "Selective epichlorohydrin-sensing performance of Ag nanoparticles decorated porous SnO_2 architectures," *CrystEngComm*, vol. 16, no. 1, pp. 110–115, 2014.

[25] A. Kolmakov, D. O. Klenov, Y. Lilach, S. Stemmer, and M. Moskovitst, "Enhanced gas sensing by individual SnO_2 nanowires and nanobelts functionalized with Pd catalyst particles," *Nano Letters*, vol. 5, no. 4, pp. 667–673, 2005.

[26] J. Cao, T. Zhang, F. Li, H. Yang, and S. Liu, "Enhanced ethanol sensing of SnO_2 hollow micro/nanofibers fabricated by coaxial electrospinning," *New Journal of Chemistry*, vol. 37, no. 7, pp. 2031–2036, 2013.

[27] Z. Li, Q. Zhao, W. Fan, and J. Zhan, "Porous SnO_2 nanospheres as sensitive gas sensors for volatile organic compounds detection," *Nanoscale*, vol. 3, no. 4, pp. 1646–1652, 2011.

[28] D. Barreca, E. Comini, A. P. Ferrucci et al., "First example of ZnO-TiO_2 nanocomposites by chemical vapor deposition: structure, morphology, composition, and gas sensing performances," *Chemistry of Materials*, vol. 19, no. 23, pp. 5642–5649, 2007.

[29] N. Hongsith, E. Wongrat, T. Kerdcharoen, and S. Choopun, "Sensor response formula for sensor based on ZnO nanostructures," *Sensors and Actuators, B: Chemical*, vol. 144, no. 1, pp. 67–72, 2010.

[30] G. Qi, L. Zhang, and Z. Yuan, "Improved H_2S gas sensing properties of ZnO nanorods decorated by a several nm ZnS thin layer," *Physical Chemistry Chemical Physics*, vol. 16, no. 26, pp. 13434–13439, 2014.

[31] C. Zhao, G. Zhang, W. Han et al., "Electrospun In_2O_3/α-Fe_2O_3 heterostructure nanotubes for highly sensitive gas sensor applications," *CrystEngComm*, vol. 15, no. 33, pp. 6491–6497, 2013.

[32] G. Han, Q. Lu, G. Liu et al., "Enhanced ethanol sensing properties based on α-Fe_2O_3/In_2O_3 hollow microspheres," *Journal of Materials Science: Materials in Electronics*, vol. 23, no. 9, pp. 1616–1620, 2012.

[33] D. Chen, X. Hou, H. Wen et al., "The enhanced alcohol-sensing response of ultrathin WO_3 nanoplates," *Nanotechnology*, vol. 21, no. 3, Article ID 035501, 2010.

[34] D. Chen, L. Yin, L. Ge et al., "Low-temperature and highly selective NO-sensing performance of WO_3 nanoplates decorated with silver nanoparticles," *Sensors and Actuators B: Chemical*, vol. 185, pp. 445–455, 2013.

[35] J. S. Lee, O. S. Kwon, D. H. Shin, and J. Jang, "WO_3 nanonodule-decorated hybrid carbon nanofibers for NO_2 gas sensor application," *Journal of Materials Chemistry A*, vol. 1, no. 32, pp. 9099–9106, 2013.

[36] C. Zhang, A. Boudiba, P. De Marco, R. Snyders, M.-G. Olivier, and M. Debliquy, "Room temperature responses of visible-light illuminated WO_3 sensors to NO_2 in sub-ppm range," *Sensors and Actuators, B: Chemical*, vol. 181, pp. 395–401, 2013.

[37] X. Wan, J. Wang, L. Zhu, and J. Tang, "Gas sensing properties of Cu_2O and its particle size and morphology-dependent gas-detection sensitivity," *Journal of Materials Chemistry A*, vol. 2, no. 33, pp. 13641–13647, 2014.

[38] L. Zhang, B. Yu, P. Ying et al., "Studies on formation mechanism of 3D Cu_2O nanospheres through self-assembly of 0D nanodots," *Superlattices and Microstructures*, vol. 84, pp. 181–191, 2015.

[39] M. Cao, C. Hu, Y. Wang, Y. Guo, C. Guo, and E. Wang, "A controllable synthetic route to Cu, Cu_2O, and CuO nanotubes and nanorods," *Chemical Communications*, no. 15, pp. 1884–1885, 2003.

[40] L. Liu, X. Zhang, and J. Chaudhuri, "Synthesis of highly nanoporous YBO_3 architecture via a co-precipitation approach and tunable luminescent properties," *Scanning*, vol. 37, no. 4, pp. 277–283, 2015.

[41] Y. Yu, L. Zhang, J. Wang et al., "Preparation of hollow porous Cu_2O microspheres and photocatalytic activity under visible light irradiation," *Nanoscale Research Letters*, vol. 7, article 347, 2012.

[42] J. Y. Xiang, J. P. Tu, Y. F. Yuan, X. H. Huang, Y. Zhou, and L. Zhang, "Improved electrochemical performances of core-shell Cu_2O/Cu composite prepared by a simple one-step method," *Electrochemistry Communications*, vol. 11, no. 2, pp. 262–265, 2009.

[43] Y. H. Du and G. J. Xu, "Hydrogen reduction of metal oxides to metals," *Atomic Energy Science and Technology*, vol. 33, p. 360, 1999.

[44] A. L. M. Reddy, S. R. Gowda, M. M. Shaijumon, and P. M. Ajayan, "Hybrid nanostructures for energy storage applications," *Advanced Materials*, vol. 24, no. 37, pp. 5045–5064, 2012.

[45] P. Meduri, C. Pendyala, V. Kumar, G. U. Sumanasekera, and M. K. Sunkara, "Hybrid tin oxide nanowires as stable and high capacity anodes for li-ion batteries," *Nano Letters*, vol. 9, no. 2, pp. 612–616, 2009.

[46] B. P. Khanal, A. Pandey, L. Li et al., "Generalized synthesis of hybrid metal-semiconductor nanostructures tunable from the

visible to the infrared," *ACS Nano*, vol. 6, no. 5, pp. 3832–3840, 2012.

[47] V. Subramanian, E. E. Wolf, and P. V. Kamat, "Catalysis with TiO_2/gold nanocomposites. Effect of metal particle size on the fermi level equilibration," *Journal of the American Chemical Society*, vol. 126, no. 15, pp. 4943–4950, 2004.

[48] X. Gou, G. Wang, J. Yang, J. Park, and D. Wexler, "Chemical synthesis, characterisation and gas sensing performance of copper oxide nanoribbons," *Journal of Materials Chemistry*, vol. 18, no. 9, pp. 965–969, 2008.

[49] D. Wang, Y. Zhen, G. Xue, F. Fu, X. Liu, and D. Li, "Synthesis of mesoporous Bi_2WO_6 architectures and their gas sensitivity to ethanol," *Journal of Materials Chemistry C*, vol. 1, no. 26, pp. 4153–4162, 2013.

[50] L. Guan, H. Pang, J. Wang, Q. Lu, J. Yin, and F. Gao, "Fabrication of novel comb-like Cu_2O nanorod-based structures through an interface etching method and their application as ethanol sensors," *Chemical Communications*, vol. 46, no. 37, pp. 7022–7024, 2010.

[51] Z. Li, Y. Zhou, J. Song, T. Yu, J. Liu, and Z. Zou, "Versatile nanobead-scaffolded N-SnO," *Journal of Materials Chemistry A*, vol. 1, no. 3, pp. 524–531, 2013.

[52] K. X. Yao, X. M. Yin, T. H. Wang, and H. C. Zeng, "Synthesis, self-assembly, disassembly, and reassembly of two types of Cu_2O nanocrystals unifaceted with 001 or 110 planes," *Journal of the American Chemical Society*, vol. 132, no. 17, pp. 6131–6144, 2010.

[53] S. Zhu, X. Liu, Z. Chen et al., "Synthesis of Cu-doped WO_3 materials with photonic structures for high performance sensors," *Journal of Materials Chemistry*, vol. 20, no. 41, pp. 9126–9132, 2010.

[54] C. Canevali, C. M. Mari, M. Mattoni et al., "Interaction of NO with nanosized Ru-, Pd-, and Pt-doped SnO_2: electron paramagnetic resonance, Mössbauer, and electrical investigation," *Journal of Physical Chemistry B*, vol. 109, no. 15, pp. 7195–7202, 2005.

[55] Y. Sui, Y. Zeng, L. Fu et al., "Low-temperature synthesis of porous hollow structured Cu_2O for photocatalytic activity and gas sensor application," *RSC Advances*, vol. 3, no. 40, pp. 18651–18660, 2013.

[56] H. Zhang, Q. Zhu, Y. Zhang, Y. Wang, L. Zhao, and B. Yu, "One-pot synthesis and hierarchical assembly of hollow Cu_2O microspheres with nanocrystals-composed porous multishell and their gas-sensing properties," *Advanced Functional Materials*, vol. 17, no. 15, pp. 2766–2771, 2007.

[57] M. Batzill and U. Diebold, "Surface studies of gas sensing metal oxides," *Physical Chemistry Chemical Physics*, vol. 9, no. 19, pp. 2307–2318, 2007.